

# Spin-polarized muons in condensed matter physics

S. J. BLUNDELL

Oxford University Department of Physics,  
Clarendon Laboratory, Parks Road, Oxford OX1 3PU

January 3, 2022

## Abstract

*A positive muon is a spin-1/2 particle. Beams of muons with all their spins polarized can be prepared and subsequently implanted in various types of condensed matter. The subsequent precession and relaxation of their spins can then be used to investigate a variety of static and dynamic effects in a sample and hence to deduce properties concerning magnetism, superconductivity and molecular dynamics. Though strictly a lepton, and behaving essentially like a heavy electron, it is convenient to think of a muon as a light proton, and it is often found with a captured electron in a hydrogen-like atom known as muonium. This article outlines the principles of various experimental techniques which involve implanted muons and describes some recent applications. The use of muons in condensed matter physics has shed new light on subjects as diverse as passivation in semiconductors, frustrated spin systems, vortex lattice melting, and quantum diffusion of light particles.*

Originally published in *Contemporary Physics* **40**, 175, (1999)

## 1 Introduction

Condensed matter physics is concerned with the properties of solids, liquids and various intermediate states of matter such as colloids (Chaikin and Lubensky 1995). From a fundamental viewpoint, all matter is made up of two main types of constituent particles, quarks and leptons (see Figure 1). The universe is composed of only these particles in addition to the gauge bosons (such as photons) which mediate forces between particles. Protons and neutrons are each made up of three quarks while electrons are thought to be indivisible and are members of a class of particle called leptons. Everyday matter, made up of protons, neutrons and electrons, is the main concern of condensed matter physics and therefore the subject arises from particles in the first column (or ‘generation’) of the standard model (Figure 1). However, more exotic particles do exist which are either more unusual leptons or combinations of more exotic quarks; they are all short-lived and have never been found to be relevant in condensed matter physics with one single exception: the muon.

The muon *is* found in nature; it is the dominant constituent of the cosmic rays arriving at sea-level and a few will be hitting you each minute as you read this article. The fact that so many muons make it

QUARKS		
u	s	t
d	c	b
LEPTONS		
e	$\mu$	$\tau$
$\nu_e$	$\nu_\mu$	$\nu_\tau$

Figure 1: Quarks ( $u$ =up,  $d$ =down,  $s$ =strange,  $c$ =charm,  $t$ =top,  $b$ =bottom) and leptons ( $e$ =electron,  $\mu$ =muon,  $\tau$ =tau, and their associated neutrinos  $\nu_e$ ,  $\nu_\mu$ ,  $\nu_\tau$ ). Everyday matter is composed of particles from the first column in this table.

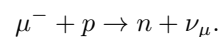
through the atmosphere is a well-known consequence of time-dilation effects in special relativity (Rossi and Hall 1941, Bailey *et al.* 1977). However, at a number of locations in the world, intense beams of muons are prepared artificially for research in condensed matter physics. In this article I will try and explain why this is done and what can be learned by firing this rather exotic ‘second-generation’ particle into various types of matter. I will describe how implanted muon studies have shed new light on problems in condensed matter physics, including those concerning semiconductors, magnetism, superconductors, and quantum diffusion. A key difference between this technique and those involving neutrons and X-rays is that scattering is *not* involved. Neutron diffraction methods use the change in energy and/or momentum of a scattered neutron to infer details about a particular sample. In contrast muons are *implanted* into a sample and reside there for the rest of their lives. The muons themselves never emerge again. It is the positrons into which they decay that are released from the sample and yield information about the muons from which they came. The experimenter plays the rôle of a coroner at an inquest; the evidence of the decay particles given up at death allows one to infer the nature of the muon’s life.

## 2 The discovery of the muon

Although the discovery of the muon is usually considered as a single event which is credited to Neddermeyer and Anderson because of their work in 1936, the story is actually more complicated and one might say that the muon slowly “emerged” over almost a half-century. Following the discovery of radioactivity in 1899, it was observed that electrometers, instruments capable of measuring the ionization produced by radioactivity, discharged even when there was no obvious radioactive source. A Jesuit priest called Thomas Wulf noticed in 1910 that this effect was more pronounced at the top of the Eiffel tower than at the bottom (Wulf 1910, see also Xu and Brown 1987). That the rate of discharge of an electrometer was an increasing function of altitude was demonstrated beyond doubt by Victor Hess in an intrepid series of ballooning experiments in the period 1911–12 (Hess 1912). He showed that electrometers discharged between three and five times faster at an altitude of 5000 m than they did at sea level. Such experiments were later extended to very high altitudes by the use of remote-controlled electrometers (in which the experimenter did not actually accompany their experiment in the balloon); this advance was achieved by Robert Millikan who was initially sceptical about Hess’ work but became rapidly convinced of its importance

(Xu and Brown 1987). Millikan’s name for the effect, *cosmic rays*, gained universal acceptance, but it was Hess who was awarded the Nobel prize for the discovery in 1936. The major constituent of cosmic rays at ground level turned out to be the muon, but the true identity of the muon remained hidden for some time.

Millikan’s group at CalTech began to perform experiments on cosmic rays at ground level by bending the rays in magnetic and electric fields. This work led to the discovery of the positron by Carl Anderson in 1932 (Anderson shared the Nobel prize in 1936 with Hess) and then the muon (initially called the *mesotron*, and later the *mu-meson*) was identified in cosmic rays by Seth Neddermeyer and Carl Anderson in 1936. They measured the mass of the muon, which turned out to be roughly one-ninth of the proton mass, and agreed extremely well with the predictions of the Japanese physicist Hideo Yukawa for a particle to mediate the strong force and hold the nucleons in the nucleus together. This result can be understood by using Heisenberg’s uncertainty principle  $\Delta E \Delta t \sim \hbar$  for this virtual particle.  $\Delta E$  is the the rest mass energy of Yukawa’s particle, the energy which has to be “borrowed”, and  $\Delta t$  is the time for it to cross the nucleus, the time for which it has to be “borrowed”; by assuming a speed  $\sim c$  for the particle one arrives at a mass  $\sim 100$  MeV, the mass found for the muon. The muon was therefore assumed to be the particle which holds the nucleus together. It took some technically difficult experiments to show that this assumption was in error and that the startling agreement with Yukawa’s predictions was misleading. Marcello Conversi, Ettore Pancini and Oreste Piccioni, working in a basement in Rome during and after the Second World War, tried to implant cosmic ray muons in matter and then measure their lifetime (Conversi *et al.* 1945, 1947). They found that positive muons implanted in anything always live on average for  $2.2 \mu\text{s}$  (the lifetime in vacuum); the lifetime of negative muons on the other hand depends on the atomic number  $Z$  of the material into which it is implanted; they measured  $2.2 \mu\text{s}$  for carbon but found  $0.07 \mu\text{s}$  for lead. They reasoned that if muons really mediated the strong force they should be gobbled up much more quickly in all materials. It appeared that muons interacted only rather weakly with matter and the only effect that was observed occurred for negative muons and turned out to be  $\mu^-$  capture:



A negative muon is attracted by atomic nuclei and since its mass is much greater than that of an electron, it readily displaces an electron from an atom and rapidly drops down to the  $1s$  state. From there it either de-

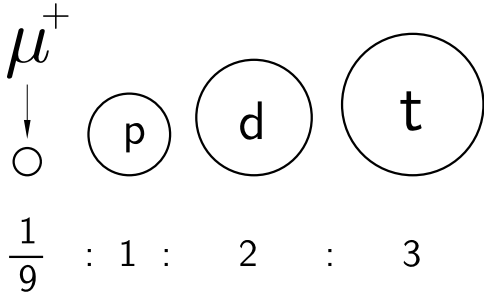


Figure 2: The muon can be considered to be the lightest member of the family of particles which include the proton, deuteron and triton. The approximate ratio of their masses are as shown. The muon thus extends the mass range of isotope substitution available to the experimenter.

cays to an electron or undergoes capture as above. The propensity to undergo capture depends on the atomic number  $Z$  (approximately as the fourth power of  $Z$ ) through the Bohr radius of the  $\mu^-$  orbit.

Yukawa's particle turned out to be the pion, discovered in cosmic rays by Powell's group in 1947 (Lattes *et al.* 1947), which decays into a muon after only  $0.026 \mu\text{s}$ , making it harder to spot in cosmic rays. Thus the muon was not a meson (a term now reserved for quark-anti-quark pairs like the pion) but a lepton, a heavy electron with no internal structure.

For experiments in condensed matter physics it is mainly the *positive* muon which is used. The negative muon  $\mu^-$ , which implants close to an atomic nucleus, is generally much less sensitive to the phenomena of interest to condensed matter physicists (magnetism, superconductivity, etc) than the site of the implanted positive muon  $\mu^+$  which sits well away from nuclei in regions of large electron density. Condensed matter physics is essentially the physics of electrons, rather than nuclei, so that the best place you can put your test particle is in the electron cloud. In fact even though the muon is a lepton (see Figure 1) and therefore essentially a heavy electron, for our purpose it is more useful to consider it as a light proton (see Figure 2).

Some properties of the electron, muon and proton are tabulated in Figure 3. The mass of the muon is intermediate between that of the electron and the proton, and thus so are its magnetic moment and gyromagnetic ratio. The latter is the constant of proportionality between angular momentum and magnetic moment.

	charge	spin	mass	moment	$\gamma / 2\pi$ (kHz $G^{-1}$ )	lifetime ( $\mu\text{s}$ )
e	$\pm e$	1/2	$m_e$ = 0.51 MeV	$657 \mu_p$	2800	$\infty$
$\mu$	$\pm e$	1/2	$207 m_e$ = 105.7 MeV	$3.18 \mu_p$	13.5	2.19
p	$\pm e$	1/2	$1836 m_e$ = 938 MeV	$\mu_p$	4.26	$\infty$

Figure 3: Properties of the electron, muon and proton.

### 3 Muon production, decay and implantation

Cosmic rays provide a major source of muons [roughly one muon arrives vertically on each square centimetre of the earth's surface every minute (Caso *et al.* 1998)] but, since the 1950s, experiments on muons have needed higher intensities and have required the development of accelerators. High energy proton beams (produced using synchrotrons or cyclotrons) are fired into a target (usually graphite) to produce pions via

$$p + p \rightarrow \pi^+ + p + n,$$

and the pions decay into muons:

$$\pi^+ \rightarrow \mu^+ + \nu_\mu,$$

where  $\nu_\mu$  is a muon-neutrino. The pion decay is a two-body decay and is therefore particularly simple. For example, consider the pions which are produced at rest in the laboratory frame. To conserve momentum, the muon and the neutrino must have equal and opposite momentum. The pion has zero spin so the muon spin must be opposite to the neutrino spin. One useful property of the neutrino is that its spin is aligned antiparallel with its momentum (it has negative helicity), and this implies that the muon-spin is similarly aligned. Thus by selecting pions which stop in the target (and which are therefore at rest when they decay) one has a means of producing a beam of 100% spin-polarized muons. This is the method most commonly used for producing muon beams for condensed matter physics research, though other configurations are in use (Brewer 1994).

The muons are stopped in the specimen of interest and decay after a time  $t$  with probability proportional to  $e^{-t/\tau_\mu}$  where  $\tau_\mu = 2.2 \mu\text{s}$  is the lifetime of the muon. The muon decay is a three body process

$$\mu^+ \rightarrow e^+ + \nu_e + \bar{\nu}_\mu$$

and so the energy of the positron  $e^+$  (which is the only particle produced in this reaction that we have a sensible hope of reliably detecting) may vary depending on

how momentum is distributed between the three particles (subject to the constraint that the total vector momentum will sum to zero, the initial momentum of the stopped muon). The decay involves the weak interaction and thus has the unusual feature of not conserving parity (Garwin *et al.* 1957). This phenomenon (which also lies behind the negative helicity of the neutrino) leads to a propensity for the emitted positron to emerge predominantly along the direction of the muon-spin when it decayed. This can be understood by considering the mirror image of the muon decay process (Figure 4).

The angular distribution of emitted positrons is shown in Figure 5 for the case of the most energetically emitted positrons. In fact positrons over a range of energies are emitted so that the net effect is something not quite as pronounced, but the effect nevertheless allows one to follow the polarization of an ensemble of precessing muons with arbitrary accuracy, providing one is willing to take data for long enough.

Muons are implanted into the sample with an energy which is at least 4 MeV. They lose energy very quickly (in 0.1–1 ns) to a few keV by ionization of atoms and scattering with electrons. Then the muon begins to undergo a series of successive electron capture and loss reactions which reduce the energy to a few hundred eV in about a picosecond. If muonium is ultimately formed then electron capture ultimately wins and the last few eV are shed by inelastic collisions between the muonium atom and the host atoms. All of these effects are very fast so that the muon (or muonium) is thermalized very rapidly. Moreover the effects are all Coulombic in origin and do not interact with the muon-spin so that the muon is thermalized in matter without appreciable depolarization. This is a crucial feature for muon-spin rotation experiments. One may be concerned that the muon may only measure a region of sample which has been subjected to radiation damage by the energetic incoming muon. This does not appear to be a problem since there is a threshold energy for vacancy production, which means that only the initial part of the muon path suffers much damage. Beyond this point of damage the muon still has sufficient energy to propagate through the sample a further distance thought to be about  $1\ \mu\text{m}$ , leaving it well away from any induced vacancies (Chappert 1984).

## 4 Spin precession and relaxation

In a magnetic field  $B$  the muon-spin precesses with angular frequency  $\omega_\mu$  given by  $\omega_\mu = \gamma_\mu B$  where  $\gamma_\mu = ge/2m_\mu$  is the gyromagnetic ratio for the muon. This is known as Larmor precession. The field-dependent

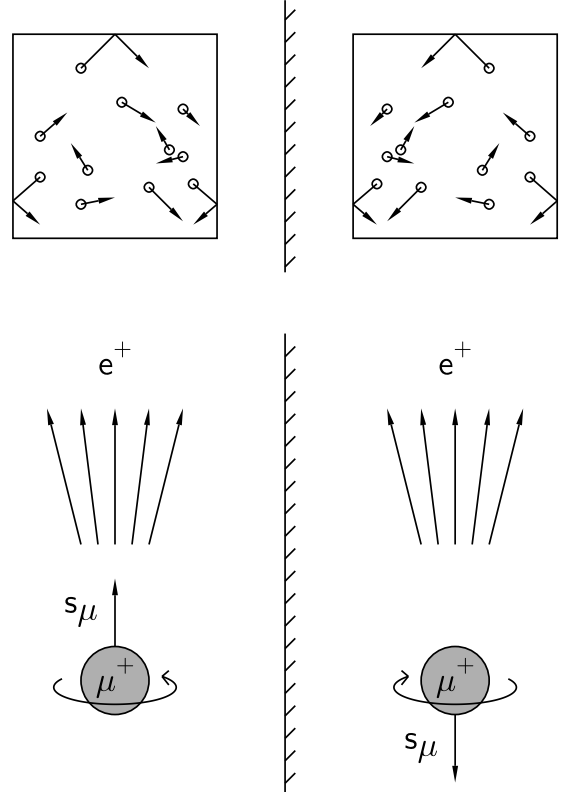


Figure 4: Top: molecules in a box collide with the walls. These collisions do not violate parity so that both the process shown on the left, and its mirror image on the right, could be observed in nature. Bottom: the same is not true for the process of muon decay. The direction of the muon-spin is reversed in the mirror so that the positrons are emitted predominantly in a direction opposite to that of the muon-spin. The violation of parity means that in our universe only the process on the left-hand side of the diagram is ever observed.

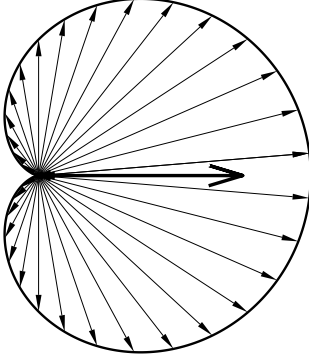


Figure 5: The angular distribution of emitted positrons with respect to the initial muon-spin direction. The figure shows the expected distribution for the most energetically emitted positrons.

precession frequencies for the muon, electron and proton are shown in Figure 6. The highest frequencies are associated with the lightest particle, the electron, and the lowest with the proton. For usual laboratory magnetic fields this explains why ESR (electron-spin resonance) is typically performed at microwave frequencies while NMR (nuclear magnetic resonance) uses radio-frequencies. In both of these techniques resonance occurs when the precession frequency matches the resonance frequency. Muon-spin rotation ( $\mu$ SR) is associated with frequencies intermediate between NMR and ESR but unlike those resonance techniques, no electromagnetic field is necessary since the precessing muon can be followed directly. [Muon-spin *resonance* experiments can however be performed (Brewer 1994) but a discussion is outside the scope of this article.]

A schematic diagram of the experiment is shown in Figure 7(a). A muon, with its polarization aligned antiparallel to its momentum, is implanted in a sample. (It is antiparallel because of the way that it was formed, see above, so the muon enters the sample with its spin pointing along the direction from which it came.) If the muon is unlucky enough to decay immediately, then it will not have time to precess and a positron will be emitted preferentially into the backward detector. If it lives a little longer it will have time to precess so that if it lives for half a revolution the resultant positron will be preferentially emitted into the forward detector. Thus the positron beam from an ensemble of precessing muons can be likened to the beam of light from a lighthouse.

The time evolution of the number of positrons detected in the forward and backward detector is described by the functions  $N_F(t)$  and  $N_B(t)$  respectively and these are shown in Figure 7(b). Because the muon

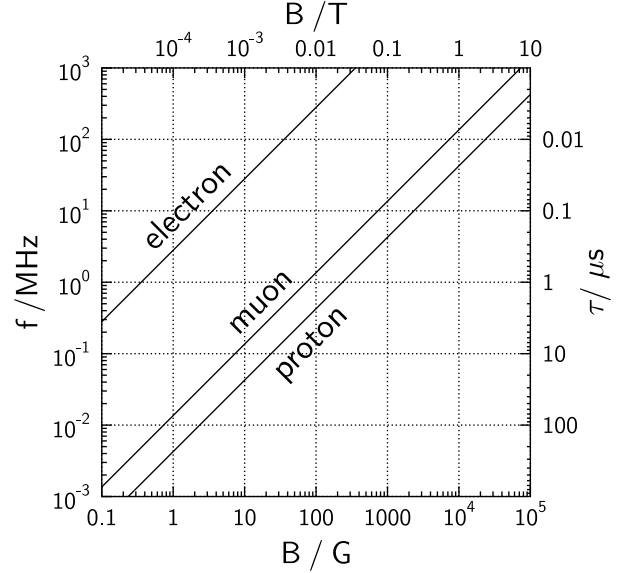


Figure 6: The Larmor precession frequency  $f$  in MHz (and the corresponding period  $\tau = 1/f$ ) for the electron, muon and proton as a function of applied magnetic field  $B$ .

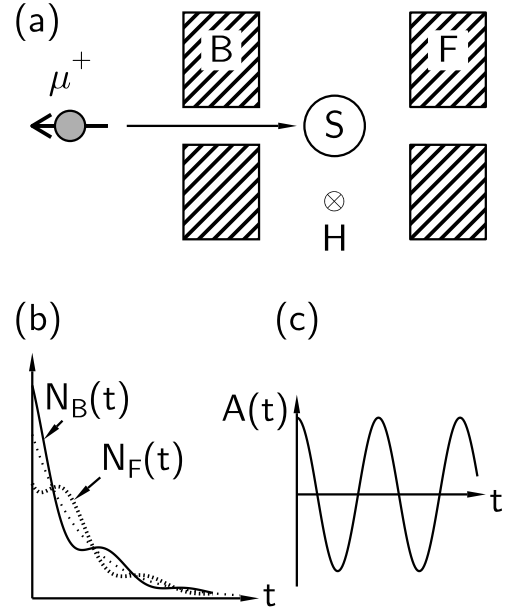


Figure 7: Schematic illustration of a  $\mu$ SR experiment. (a) A spin-polarized beam of muons is implanted in a sample  $S$ . Following decay, positrons are detected in either a forward detector  $F$  or a backward detector  $B$ . If a transverse magnetic field  $H$  is applied to the sample as shown then the muons will precess. (b) The number of positrons detected in the forward and backward detectors. (c) The asymmetry function.

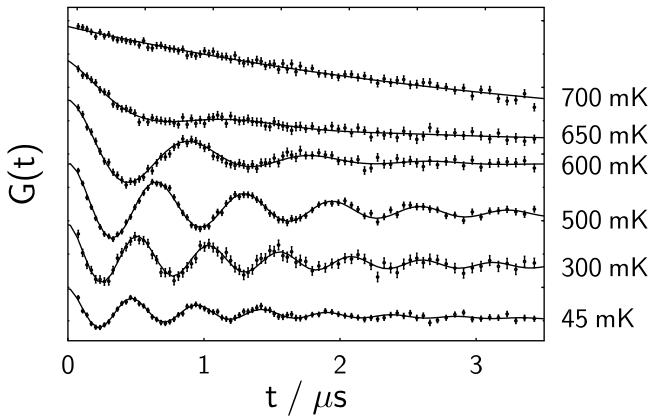


Figure 8: Zero-field muon spin rotation frequency in the organic ferromagnet *p*-NPNN (Blundell *et al.* 1995).

decay is a radioactive process these two terms sum to an exponential decay. Thus the time evolution of the muon polarization can be obtained by examining the normalized difference of these two functions via the asymmetry function  $A(t)$ , given by

$$A(t) = \frac{N_B(t) - N_F(t)}{N_B(t) + N_F(t)}, \quad (1)$$

and is shown in Figure 7(c).

This experimentally obtained asymmetry function has a calculable maximum value,  $A_{\max}$ , for a particular experimental configuration which depends on the initial beam polarization (usually very close to 1), the intrinsic asymmetry of the weak decay, and the efficiency of the detectors for positrons of different energies, and usually turns out to be around  $A_{\max} \sim 0.25$ . The function can be normalized to 1, in which case it expresses the spin autocorrelation function of the muon,  $G(t) = A(t)/A_{\max}$ , which represents the time-dependent spin polarization of the muon.

A magnetic field does not need to be applied for the muons to precess if the sample has its own magnetic field. Figure 8 shows muon-spin rotation data for muons implanted into an organic ferromagnet (Blundell *et al.* 1995). This material magnetically orders only at very low temperatures ( $T_C = 0.67$  K) so that experiments must be carried out in a dilution refrigerator. This presents no problems for the muon which passes through the windows of the cryostat and implants in the sample, revealing the internal magnetisation. As the sample is warmed, the frequency of oscillations decreases as the internal field decreases until it is above the Curie temperature and no oscillations can be observed, only a weak spin relaxation arising from spin fluctuations.

This is an example of an experiment with no applied magnetic field (in fact a small magnetic field was applied to compensate the effect of the earth's field). Very often magnetic fields are applied to the sample either perpendicular or parallel to the initial muon-spin direction. The perpendicular (or transverse) case causes the muon to precess in the applied magnetic field and any dephasing in the observed oscillations is evidence for either an inhomogeneous internal field distribution or spin-spin ( $T_2$  in the language of NMR) relaxation. The parallel (or longitudinal) case will be described in more detail later and does not lead to spin precession, but spin relaxation. This can be due to inhomogeneous field distributions or spin-lattice ( $T_1$ ) relaxation processes.

Muon experiments can be performed in two different ways depending on the time structure of the muon beam. If the muon beam is continuous (CW, or continuous wave see Figure 9(a)), then muons arrive at the sample intermittently. When the muon enters the experiment it must itself be detected to start a clock. When the positron is detected in either the forward or backward detectors, the clock is stopped. If a second muon arrives before the first one has decayed then one has no way of knowing whether a subsequently emitted positron came from the first or second muon, so this event must be disregarded. Sophisticated high-speed electronics and a low incident muon arrival rate are needed. Alternatively one can use an electrostatic deflector triggered by the detectors to ensure no muons enter the experiment until the current implanted muon decays.

These complications are circumvented with a pulsed muon beam (Figure 9(b)). In this case a large number of muons arrive in a very intense pulse so there is no need to detect when each muon arrives. The detection of positrons is then made and each event is timed with respect to the arrival of the pulse. A typical dataset contains several million detected positrons so that an appreciable number of muons (the fraction is given by  $e^{-20/2.2} \sim 0.01\%$ ) live for 20  $\mu$ s or longer. Long-lived muons are difficult to measure with CW beams; the arrival of the next muon tends to interrupt the first muon which has outstayed its welcome! Nevertheless the long-lived muons can be accurately detected at a pulsed source. Unfortunately this method also suffers from a drawback which is that the muon pulse has a finite width,  $\tau_w$ , which results in a slight ambiguity in all of the timing measurements and leads to an upper limit on precession frequencies which can be measured. By the standard of other unstable elementary particles, the muon is comparatively long-lived with a lifetime of  $\tau = 2.2$   $\mu$ s. CW muon beams are operated at the Paul

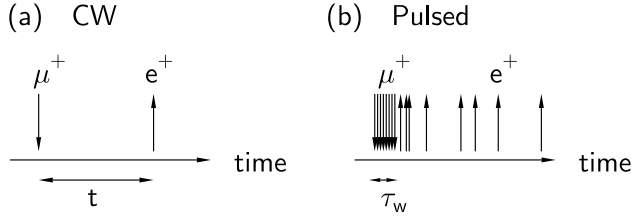


Figure 9: Schematic illustration of the two types of muon beam (a) continuous wave (CW) and (b) pulsed.

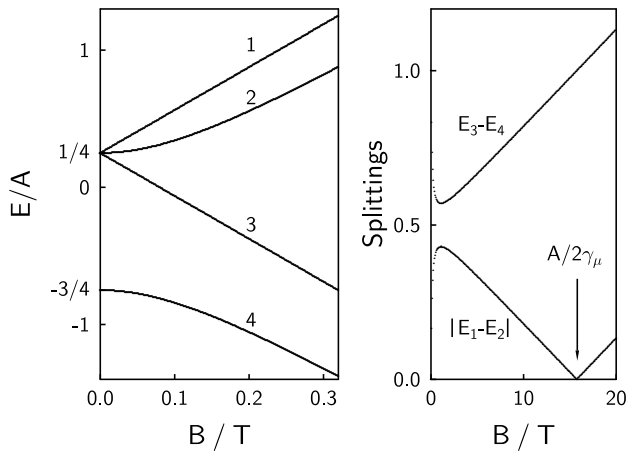


Figure 10: The Breit-Rabi diagram for isotropic muonium with a hyperfine constant  $A = 4463$  MHz appropriate for free (vacuum) muonium. Also shown are the splittings between pairs of levels over a larger range of magnetic field. Levels 1 and 2 cross at a field of  $\sim 16.5$  T for free muonium.

Scherrer Institute in Switzerland and at TRIUMF in Canada. Pulsed muon beams are used at KEK in Japan and at ISIS (the spallation source at the Rutherford Appleton Laboratory) in the UK.

## 5 Muonium

Depending on its chemical environment, the muon can thermalize and pick up an electron and form a neutral atomic state called muonium (abbreviated  $\text{Mu} = \mu^+ e^-$ ) which is an analogue of atomic hydrogen. In muonium the electronic spin and the muon-spin are coupled by a hyperfine interaction which we will initially assume is isotropic. This leads to two energy levels, a lower triplet state and a higher singlet state. In a magnetic field the triplet levels split and the energy levels move as shown in the Breit-Rabi diagram in Figure 10.

Isolated hydrogen or muonium is one of the simplest

defects in a semiconductor. The electronic structures of analogous hydrogen and muonium centres are expected to be identical, apart from vibrational effects reflecting their difference in mass. If muons are implanted into a semiconductor like silicon, neutral muonium tends to form at the tetrahedral sites (labelled  $T$  in Figure 11) and can diffuse rapidly between such sites. The electronic state is isotropic and in a transverse-field experiment the transitions between energy levels can be observed as precession frequencies  $\nu_{ij}$  equal to the splitting between energy levels  $(E_i - E_j)/h$  (as shown in Figure 10). The strength of the hyperfine interaction in semiconductors is usually close to half that of the vacuum value (the reduction is due to some admixture of the electron spin density with surrounding atoms). However, a substantial fraction of neutral muonium is also found in a most unexpected place, wedged into the centre of a stretched Si-Si bond (the site is labelled  $BC$  in Figure 11 for ‘bond-centre’, see Patterson 1988 for a review of muonium states in semiconductors). This state is extremely immobile, and surprisingly turns out to be the thermodynamically more stable site. Its hyperfine coupling is much lower than that of the tetrahedral state, typically less than 10% of the vacuum value. Furthermore the coupling is very anisotropic, with axial symmetry about the  $\langle 111 \rangle$  crystal axis (i.e. along the Si-Si bonds), so that the energy levels behave in a different manner to that indicated in Figure 10. These states have rather interesting dynamics and can undergo charge and spin exchange processes, cycling rapidly between positive and negative charge states via interaction with conduction electrons (Chow *et al.* 1994). The characterisation of all these states is important because it is found that atomic hydrogen is present in most semiconductors and is able to passivate (i.e. deactivate) the dangling bonds in amorphous silicon allowing it to show semiconducting properties. Hydrogen is inevitably present in all semiconductors, often becoming incorporated during material production from hydride gases or during etching, but the low concentration makes direct spectroscopic studies very difficult. Using muonium (albeit in the ultra-dilute limit!) as an analogue for hydrogen has therefore been a promising method of obtaining a great deal of spectroscopic information concerning this problem.

Muonium states can also be formed in many chemical systems and allow a unique form of radical spectroscopy (Roduner 1993). Muonium adds to unsaturated bonds to form muonated free radicals. For example, addition to benzene ( $\text{C}_6\text{H}_6$ ) leads to the muonated cyclohexadienyl radical ( $\text{C}_6\text{H}_6\text{Mu}$ ). The advantage here is that one can work with concentrations down to just one muonated radical at a time in an entire sample. In con-

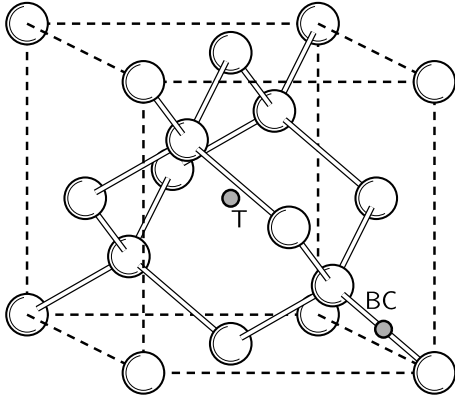


Figure 11: The crystal structure of silicon, showing the possible muonium sites (T=tetrahedral site, BC=bond-centre site).

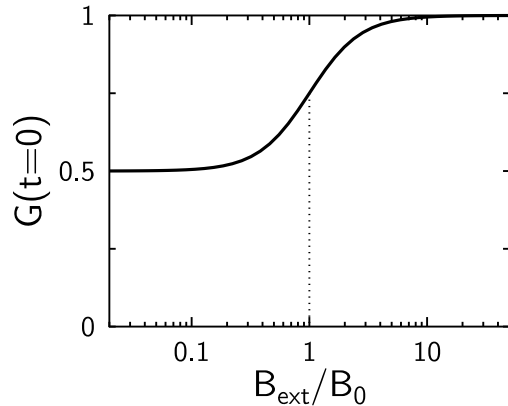


Figure 12: Repolarization of the initial muon polarization.

trast ESR detection needs  $\sim 10^{12}$  radicals in a cavity, forbidding measurements at high temperatures where the radicals become mobile and terminate by combination. The technique has been applied to radicals in various environments (Roduner 1993) including those absorbed on surfaces (Reid *et al.* 1990).

In all cases the muonium can be studied by measuring precession signals in an applied magnetic field, or by using a technique known as repolarization (Figure 12). In this latter method a longitudinal magnetic field is applied to the sample, along the initial muon-spin direction, and as the strength of the magnetic field increases, the muon and electron spins are progressively decoupled from the hyperfine field. For isotropic muonium, half of the initial polarization of implanted muons is lost because of the hyperfine coupling, but this is recovered in a sufficiently large applied field (Figure 12), allowing an estimate of the strength of the hyperfine field. If the hyperfine coupling is anisotropic then this affects the form of the repolarization curve, allowing

further information to be extracted (Pratt 1997).

At very high fields, when the electron and muon spins are completely decoupled, the initial muon polarization is preserved. However, at certain values of the magnetic field a level-crossing of energy levels may occur. In fact, there is one at very high field in vacuum muonium (see Figure 10(b)). Interactions between the muon-electron system and nuclei in the host material cause the pure Zeeman states to mix near these level-crossings, thereby avoiding the crossing, and this can lead to a loss of polarization. This provides a further technique to extract hyperfine coupling strengths and also measurements of quadrupole couplings (Cox 1987, Roduner 1993, Brewer 1994). It turns out that these avoided-level-crossing resonances are also a sensitive probe of dynamics and this technique has been applied to a number of studies of molecular motion (Roduner 1993).

An interesting situation occurs in the case of  $C_{60}$  in which muonium can implant inside the buckyball cage (this state is called endohedral muonium). The unpaired electron part of the muonium greatly enhances the sensitivity to scattering from conduction electrons so that this state is extremely useful for studying alkali-fulleride superconductors (MacFarlane *et al.* 1998). It is also possible to form a muonium radical by external addition, essentially muonium attacking the outside of a buckyball, breaking a double bond and ending up covalently bonded to a single saturated carbon atom. This centre is very sensitive to the molecular dynamics of the local environment and has been used to extract the correlation time for molecular reorientation (Kiefl *et al.* 1992).

In metallic samples the muon's positive charge is screened by conduction electrons which form a cloud around the muon, of size given by a Bohr radius. Thus  $\mu^+$ , rather than muonium, is the appropriate particle to consider in a metal. (The endohedral muonium found in alkali fulleride superconductors is the only known example of a muonium state in a metal.) In insulators and semiconductors screening cannot take place so that the muon is often observed in these systems either as muonium or is found to be chemically bound to one of the constituents, particularly to oxygen if it is present. Isotropic muonium states are found in many semiconducting and insulating systems. The value of the hyperfine coupling strength is close to that for vacuum (free) muonium if the band gap is large. For materials with smaller band gap the hyperfine coupling is lower reflecting the greater delocalization of the electron spin density on to neighbouring atoms (Cox 1987).



## 6 Muons and magnetism

Muons are ideally suited to studying problems in magnetism. Implanted muons in magnetically ordered materials precess in the internal magnetic field and directly yield signals proportional to that magnetic field. In this respect the muon behaves as a microscopic magnetometer. The very large magnetic moment of the muon makes it very sensitive to extremely small magnetic fields (down to  $\sim 10^{-5}$  T) and thus is very useful in studying small moment magnetism. It is also valuable in studying materials where the magnetic order is random or of very short range. Since muons stop uniformly throughout a sample, each signal appears in the experimental spectrum with a strength proportional to its volume fraction, and thus the technique is helpful in cases where samples may be multiphase or incompletely ordered. Because no spatial information is obtained (in contrast to diffraction techniques) single crystal samples are not essential (though they can be useful in certain cases) and experiments can often provide information on the magnetic order of certain materials where conventional magnetic neutron diffraction cannot be simply performed.

The most straightforward application of the technique is to ferromagnets and antiferromagnets in which cases the muon is used to follow the temperature dependence of the internal field and to extract critical exponents (Schenck and Gyax 1995). An example of this type of experiment has already been presented in Figure 8. The internal field at the muon site is due to a sum of the applied field (if used), the dipolar and demagnetization fields (which can be calculated from the magnetization) and the hyperfine field induced by the applied field. To extract quantitative information from  $\mu$ SR experiments it is necessary to know the muon-site and this can in some cases hinder the search for a straightforward interpretation of the data. Usually there are a small set of possible interstitial sites which the muon can occupy and in favourable circumstances only one will be consistent with the observed data. Nevertheless the technique has been widely applied to magnetic materials (Schenck and Gyax 1995, Dalmas de Réotier and Yaouanc 1997) and has found great applicability to the study of heavy fermion systems (Amato 1997). These latter materials are based on rare-earth and actinide elements and show strong electronic correlations between localized  $f$  moments and conduction electrons. They exhibit a subtle competition between the Kondo effect (by which magnetic moments are ‘mopped up’ by the screening spin polarization of conduction electrons) and the magnetic Ruderman-Kittel-Kasuya-Yosida (RKKY) interactions

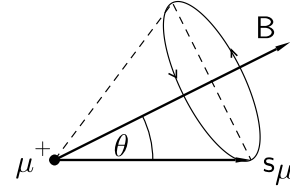


Figure 13: Muon-spin precession with a magnetic field  $B$  applied at an angle  $\theta$ .

(which couple magnetic moments through the conduction electrons). Depending on the relative strength of these effects, magnetic order can be observed at low temperature but it is often incommensurate or random and can be associated with very small static moments. The sensitivity of the muon to tiny fields and the absence of a muon quadrupolar moment (which can complicate analogous NMR experiments) has led to muons being extensively utilised in this field (Amato 1997).

To understand the ability of the muon to study randomness and dynamics in magnetism it is helpful to consider further some aspects of spin precession. If the local magnetic field at the muon-site is at an angle of  $\theta$  to the initial muon spin-direction at the moment of implantation, the muon-spin will subsequently precess around the end of a cone of semi-angle  $\theta$  about the magnetic field (Figure 13). The normalized decay positron asymmetry will be given by

$$G(t) = \cos^2 \theta + \sin^2 \theta \cos(\gamma_\mu B t). \quad (2)$$

If the direction of the local magnetic field is entirely random then averaging over all directions would yield

$$G(t) = \frac{1}{3} + \frac{2}{3} \cos(\gamma_\mu B t). \quad (3)$$

If the strength of the local magnetic field is taken from a Gaussian distribution of width  $\Delta/\gamma_\mu$  centred around zero, then a straightforward averaging over this distribution gives

$$G(t) = \frac{1}{3} + \frac{2}{3} e^{-\Delta^2 t^2 / 2} (1 - \Delta^2 t^2), \quad (4)$$

a result which was first obtained by Kubo and Toyabe (Kubo and Toyabe 1967) as an entirely theoretical exercise. This relaxation function is illustrated in Figure 14(b). Its origin is indicated schematically in Figure 14(a) which shows a number of curves of equation 4 for different values of the internal field  $B$ . Initially they all do roughly the same thing (i.e. fall from 1 to a minimum value and then increase) but after a short time they dephase with respect to each other. Hence their average, the Kubo and Toyabe relaxation

function, would be expected to fall from unity to a minimum and then recover to an average value, in this case to one-third.

This relaxation function is often observed experimentally, for example in experiments on copper at 50 K with zero applied field (Luke *et al.* 1991). At this temperature the muon is stationary and precesses in the field due to the neighbouring nuclear dipoles which are randomly orientated with respect to each other and give rise to a field distribution each component of which is Gaussian distributed about zero. (At higher temperatures this is not seen because of thermally activated muon hopping while at lower temperatures an effect known as quantum diffusion may occur, see section 8.)

If the form of the distribution of internal fields was different then this would affect the form of the observed muon-spin time evolution. For example, in a material with a spin-density wave which is incommensurate with the crystal lattice, there will be a sinusoidal modulation of the internal field which the muons will randomly sample. In this case one finds that the muon-spin relaxation follows a Bessel function (Major *et al.* 1986, Amato 1997). Such an effect has been observed in chromium (Major *et al.* 1986) and also in an organic system, (TMTSF)<sub>2</sub>PF<sub>6</sub>, which exhibits a spin-density wave ground state (Le *et al.* 1993).

If there is an almost uniform static internal field in the sample, but there is a slight variation from site to site, different muons will precess at slightly different frequencies and become progressively dephased so that the oscillations in the data will be damped. If the field varies a great deal the damping could be so large that no oscillations can be observed. However this effect could also be caused by fluctuations either of the internal field, because of some intrinsic property of the sample, of the muon's position, or because of muon diffusion. One method of distinguishing between these possibilities is to apply a magnetic field in the longitudinal direction, parallel to the initial muon-spin direction. For example, this modifies the Kubo-Toyabe relaxation function as shown in Figure 14(c), causing the “ $\frac{1}{3}$ -tail” to increase since in this case the muons precess in both the internal field and the applied field. Since the magnetic field  $B_L$  is applied along the initial muon-spin direction then in the limit of large  $B_L$  the muon-spin is held constant and does not relax from a value near unity. This technique is useful to distinguish the effects of inhomogeneous line broadening (a distribution of static internal fields as considered above) and fluctuations because the two have very different behaviours in a longitudinal field (Hayano *et al.* 1979).

The effects of muon hopping on the relaxation are shown in Figure 15. The different traces are for dif-

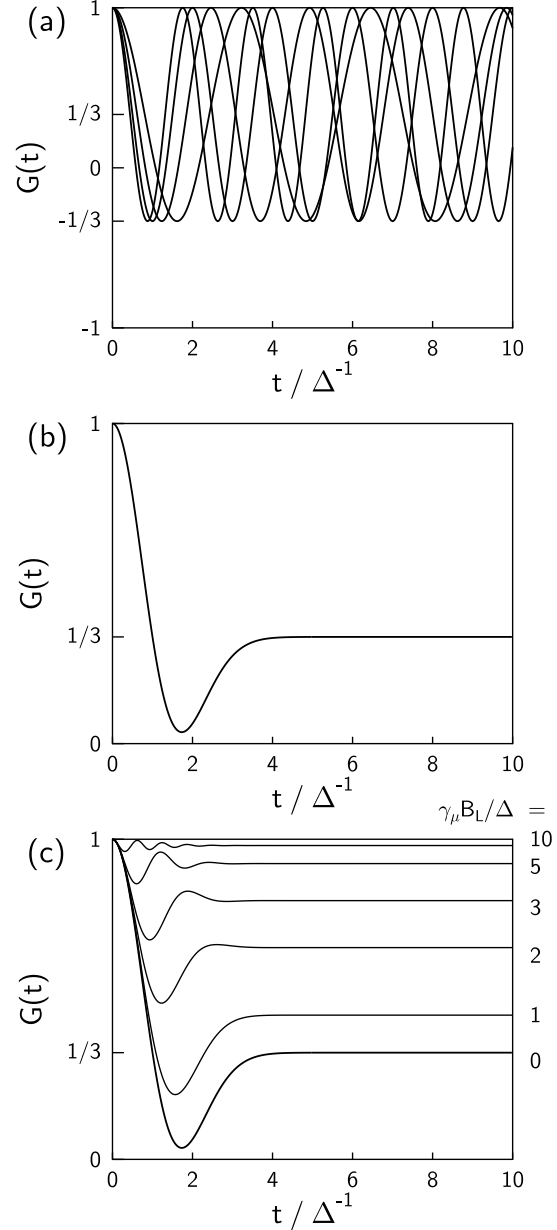


Figure 14: (a) The time evolution of the muon-spin polarization for equation 3 with different values of the magnitude of the local field  $|B|$ . (b) The averaging of terms from (a) yields the Kubo-Toyabe relaxation function (equation 4) with its characteristic dip and recovery to a value of  $1/3$ . (c) The effect of a longitudinal magnetic field  $B_L$ . The time is measured in units of  $\Delta^{-1}$  and the longitudinal field values shown are in units of  $\Delta/\gamma_\mu$ .

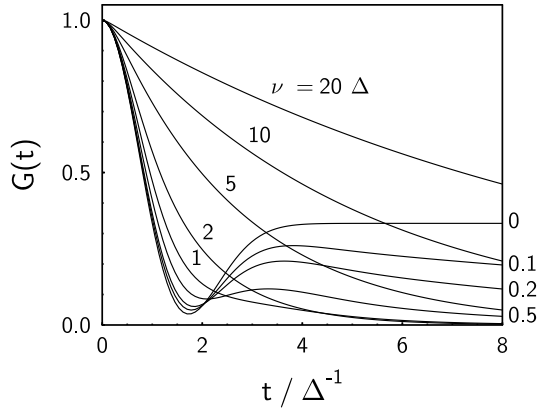


Figure 15: The relaxation function for a muon hopping at rate  $\nu$ . After each hop the value of the internal field is taken from a Gaussian distribution about zero with width  $\Delta/\gamma_\mu$ . The curve for  $\nu = 0$  corresponds to the zero-field Kubo-Toyabe relaxation function of equation 4.

ferent hopping rates  $\nu$ . When  $\nu = 0$  we recover the zero-field Kubo-Toyabe curve of equation 4. For fast hopping the relaxation of the muon-spin becomes dominated by the hopping process and the relaxation is exponential. The relaxation rate goes down as the dynamics get faster. This effect is known as motional narrowing because it is essentially identical to the effect of the same name in NMR spectroscopy. Motional effects narrow NMR linewidths which are measured in the frequency domain; consequently in the time domain (in which data from  $\mu$ SR experiments are usually considered) this corresponds to a motional widening and a reduction in relaxation.

For slow hopping, very little effect is observed at very short times but a large sensitivity to weak hopping is observed in the  $\frac{1}{3}$ -tail which is observed at longer times. This sensitivity to slow dynamics via the behaviour of the tail of the relaxation function observed at long times permits a measurement of dynamics over a very large range of time scale.

If a longitudinal magnetic field is applied then it has a large effect on the muon relaxation if the dynamics are weak but much less of an effect if the dynamics are fast. Thus by a careful combination of zero-field and longitudinal-field experiments the nature of the internal field distribution can be extracted.

Such an analysis has been done for many systems in which the issue of the presence of dynamics and/or magnetic order has profound consequences. A good example is that of the spin ladder cuprates (Kojima *et al.* 1995).  $\text{Sr}_2\text{Cu}_4\text{O}_6$  has a crystal structure such that  $\text{Cu}^{2+}$  spins are arranged in weakly coupled 2-leg lad-

ders.  $\mu$ SR experiments show no magnetic order down to very low temperatures.  $\text{Sr}_4\text{Cu}_6\text{O}_{10}$  is a 3-leg ladder and  $\mu$ SR finds static magnetic order appearing at  $\sim 52$  K. This is consistent with theoretical predictions of a non-magnetic ground state in even-leg-number systems (due to the formation of spin-singlets between pairs of spins on each rung) but a magnetic ground state in odd-leg-number systems (Kojima *et al.* 1995). Similar types of experiments have been performed on  $\text{SrCr}_8\text{Ga}_4\text{O}_{19}$ , a material which has magnetic moments lying in an arrangement known as a Kagomé lattice which is highly frustrated in the sense that there is no unique ground state. These measurements have demonstrated the presence of dynamic spin fluctuations which persist down to at least 0.1 K (Uemura *et al.* 1994). These strong dynamics which remain at very low temperatures are characteristic of a spin-liquid state in which a small number of unpaired spins migrate in a sea of singlet pairs. Some compounds with one-dimensional chains of antiferromagnetically coupled spins can show an effect known as the spin-Peierls transition. Below a transition temperature the chain dimerises, pairing alternate spins into singlets and opening up a gap in the excitation spectrum, drastically changing the dynamics.  $\mu$ SR studies have been performed on both inorganic and organic systems which show this effect (Lappas *et al.* 1994, Blundell *et al.* 1997).

A celebrated example of a frustrated spin system is a spin glass, such as the dilute alloy spin glass prepared by dissolving small concentrations of Mn in a Cu matrix. In these system dilute magnetic impurities couple via an RKKY exchange interaction which alternates in sign as a function of distance. Because the magnetic impurities are present at random, these materials cannot show long range order but have built-in frustration. When cooled one observes a slowing down of spin fluctuations and a divergence in the correlation time between Mn spin fluctuations at the spin glass temperature. Below this temperature, a static component of the local field is observed with muons, corresponding to some degree of spin freezing, with each Mn spin having its own preferred orientation, although fluctuating around this (Uemura *et al.* 1985). Above the spin glass temperature muon-spin relaxation measurements have been used to follow the spin glass dynamics and to directly extract the form of the autocorrelation function of the spins (Campbell *et al.* 1994, Keren *et al.* 1996).

An interesting situation occurs when a muon hops in an antiferromagnetically ordered lattice. With no hopping, and if there is one muon site close to each spin in the system, there will be a single precession frequency. Because the sign of the internal field reverses every time the muon hops, the muon will precess one way and then,

after hopping, precess back again. As the hop rate increases the oscillations are progressively destroyed until eventually no relaxation is possible (Keren *et al.* 1993). This effect has been observed experimentally in the cuprate compound  $\text{Ca}_{0.86}\text{Sr}_{0.14}\text{CuO}_2$  (Keren *et al.* 1993).

## 7 Muons and superconductivity

One of the most fruitful areas of recent research with muons has been in the area of superconductivity. The last couple of decades have witnessed a renaissance in this field following the discovery of high-temperature superconductors, organic superconductors, borocarbide superconductors, and even superconductors based on  $\text{C}_{60}$  buckyballs. To understand the usefulness of muons, recall that the two important lengthscales in superconductors are the penetration depth,  $\lambda$ , which controls the ability of the superconductor to screen magnetic fields, and the coherence length,  $\xi$ , which controls the length-scale over which the order parameter can vary without undue energy cost. If the former is sufficiently greater than the latter (the condition is that  $\lambda > \xi/\sqrt{2}$ ) the material is a type II superconductor which if cooled through its transition temperature,  $T_c$ , in an applied magnetic field remains superconducting everywhere except in the cores of the superconducting vortices which usually are arranged in a triangular lattice. Each vortex is associated with a magnetic flux equal to one flux quantum  $\Phi_0 = h/2e$ . The distance between vortices,  $d$ , is such that the number of vortices per unit area  $2/\sqrt{3}d^2$  equals the number of flux quanta per unit area  $B/\Phi_0$ . Thus  $d \propto B^{-1/2}$ . In general the vortex lattice will be incommensurate with the crystal lattice and, except at very high magnetic field, the vortex cores will be separated by a much larger distance than the unit-cell dimensions. Implanted muons will sit at certain crystallographic sites and thus will randomly sample the field distribution of the vortex lattice.

In the normal state ( $T > T_c$ ) with a transverse field  $B$ , all muons precess with frequency  $\omega = \gamma_\mu B$  (Figure 16(a)). In the superconducting state however the muons implanted close to the vortex cores experience a larger magnetic field than those implanted between vortices. Consequently there is a spread in precession frequency, resulting in a progressive dephasing of the observed precession signal (Figure 16(b)). The larger the penetration depth, the smaller the magnetic field variation and the less pronounced the dephasing (compare Figure 16(b) and (c)). It turns out that this idea can be quantified (see Aegerter and Lee 1997) and that the relaxation rate  $\sigma$  of the observed precession signal

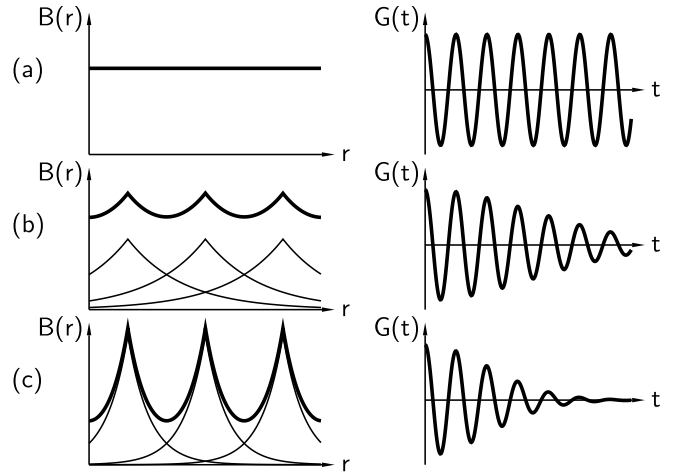


Figure 16: The field distribution inside a superconductor as a function of position and the corresponding muon-spin relaxation function for three cases: (a) the normal state, (b) the superconducting state, (c) as (b) but with a shorter penetration depth.

is related to the penetration depth using

$$\sigma = \gamma_\mu \langle B(\mathbf{r}) - \langle B(\mathbf{r}) \rangle_{\mathbf{r}} \rangle_{\mathbf{r}}^{1/2} \approx 0.0609 \gamma_\mu \Phi_0 / \lambda^2, \quad (5)$$

where  $B(\mathbf{r})$  is the field at position  $\mathbf{r}$  and the averages are taken over all positions. Thus the relaxation rate of the observed precession signal can be used to directly obtain the magnetic penetration depth. An advantage is that data are obtained from the bulk of the superconductor, in contrast to techniques involving microwaves which are only sensitive to effects at the surface.

This principle has been applied to many different superconductors to extract both the penetration depth and its temperature dependence. This latter quantity is of great interest because it is a measure of the temperature dependence of the order parameter and can yield information concerning the symmetry of superconducting gap and hence the symmetry of the pairing mechanism. For example this approach has revealed unconventional pairing in a sample of the high temperature superconductor  $\text{YBa}_2\text{Cu}_3\text{O}_{6.95}$  (Sonier *et al.* 1994). It is also possible to extract the vortex-core radius from a detailed analysis of the data (Yaouanc *et al.* 1997, Sonier *et al.* 1997).

A conventional type II superconductor exhibits 3 well-defined phases for  $T < T_c$ : (1) a Meissner phase for  $B < B_{c1}$ , (2) a mixed or Shubnikov phase for  $B_{c1} < B < B_{c2}$  (in which the magnetic field enters the superconductor in the form of well defined flux lines or vortices arranged in a lattice) and (3) the normal metal-

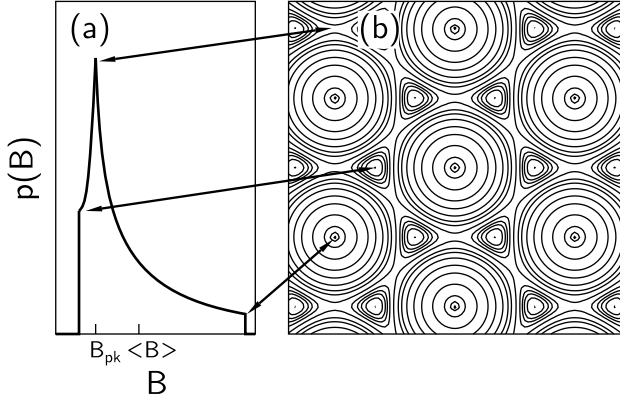


Figure 17: (a) The field distribution  $p(B)$  in the vortex lattice (contours of  $B$  shown in (b)).

lic phase for  $B > B_{c2}$ . In highly anisotropic systems the vortex lattice is no longer a system of rigid rods but should be considered as a system of flexible interacting lines. A useful picture is that of a weakly coupled stack of quasi-two-dimensional (q2D) “pancake” vortices, each one confined to a superconducting plane (Blatter *et al.* 1995, Clem 1991). The phase diagram is thus substantially altered to take account of field and temperature dependent changes in the vortex lattice itself. At low  $T$  and low  $B$  the stacks resemble conventional vortex lines. Above a characteristic temperature  $T_b$ , but still below that at which superconductivity is destroyed, the vortex lattice is broken up by thermal fluctuations (Clem 1991) (this is called vortex lattice melting). At low  $T$ , but this time increasing  $B$ , the energetic cost of interlayer deformations of the lattice (local tilting of the lines) is progressively outweighed by the cost of intralayer deformations within the superconducting plane (shearing). Above a crossover field  $B_{cr}$  the vortex lattice enters a more two-dimensional regime. Thus in anisotropic systems we may expect temperature and field dependent transitions in which the vortex lattice is destroyed. When muons are implanted into a superconductor in a field  $B_{\text{applied}}$  one can directly measure the field distribution  $p(B)$  which is given by  $p(B) = \langle \delta(B - B(\mathbf{r})) \rangle_{\mathbf{r}}$  and is the probability that a randomly chosen point in the sample has field  $B'$  (Brandt 1988, Aegerter and Lee 1997). This is shown in Fig. 17(a) for an ideal vortex line lattice. The distribution is highly asymmetric, the high field “tail” corresponding to regions of the lattice close to the vortex cores (see Fig. 17(b)). The maximum of the distribution occurs at  $B_{pk}$ , which lies below the mean field  $\langle B \rangle$  (see Fig. 17(a)). Such lineshapes have been observed at low temperatures and fields in vari-

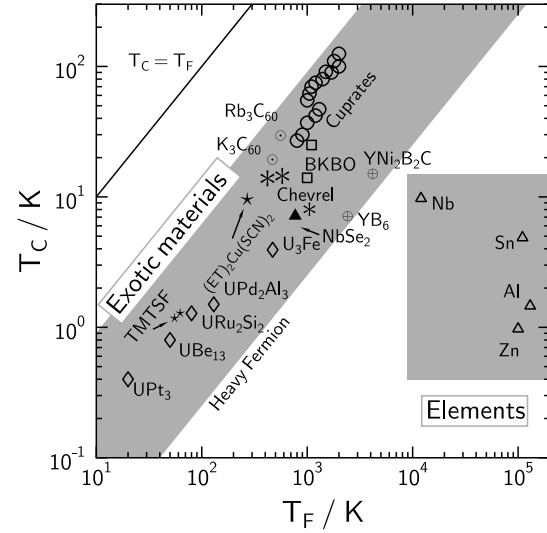


Figure 18: The Uemura plot, showing the correlation between the superconducting transition temperature  $T_c$  and the Fermi temperature  $T_F$ . The exotic superconductors fall within a common band. Adapted from Uemura *et al.* 1991 and Hillier and Cywinski 1997.

ous anisotropic superconductors using  $\mu$ SR, including the high temperature superconductors (Lee *et al.* 1993, Aegerter and Lee 1997) and also in organic superconductors (Lee *et al.* 1997). In both case it is found that the vortex lattice can be melted with temperature at  $T_b$  or can cross into a two-dimensional regime at fields above  $B_{cr}$ . Both transitions can be followed by measuring the field and temperature dependence of the  $p(B)$  line shapes.

The London formula for the zero temperature limit of the penetration depth  $\lambda(0)$  yields in the clean limit (the mean free path much bigger than the coherence length) the relation:  $\lambda(0) \propto \sqrt{m^*/n_s(0)}$  where  $m^*$  is the effective mass and  $n_s(0)$  is the density of superconducting electrons. This can be combined with measurements of the Sommerfeld constant to yield a value for the Fermi temperature  $T_F$ . Thus from muon measurements it is possible to plot a diagram showing the relationship between the Fermi and critical temperatures for a range of superconductors (Uemura *et al.* 1991). This picture (see Figure 18) has come to be called a Uemura plot and shows a clear correlation between  $T_c$  and  $T_F$  for the heavy fermion, organic, fullerene and Chevrel phase superconductors. The conventional, elemental superconductors lie away from this correlation and have values of  $T_c/T_F \sim 10^{-3}$  (for the “exotic” superconductors this value is one or two orders of magnitude larger). This correlation has been interpreted as evidence that the exotic superconductors may be close to Bose-Einstein

condensation which is expected to occur at a temperature  $\sim T_F$  (Uemura *et al.* 1991). Whether or not this speculation is correct, it is expected that this remarkable correlation should constrain theories to explain the superconductivity in these various exotic systems and is possibly suggestive of a common mechanism lying behind them.

## 8 Muons as active probes

In almost everything we have considered so far we have been tacitly assuming that the muon is a passive probe and does not disturb its surroundings. If it has been sensitive to dynamics, we have believed that the muon takes no part in them itself. This in fact is very often true. However, there are a number of situations in which the muon plays an active rôle. For example, at high temperature in copper the muon diffuses from interstitial site to interstitial site. In this case the major component of the observed depolarization is due to the muon motion. In semiconductors the muonium can undergo charge and spin exchange with conduction electrons and thereby one measures dynamics with which the muon itself is intimately involved.

An extreme case where the muon plays a strongly active rôle is found in conducting polymers (Hayes 1995). Figure 19 shows the reaction between muonium and trans-polyacetylene (Nagamine *et al.* 1984) which produces a diamagnetic, neutral muon defect and a highly mobile unpaired spin. This soliton diffuses up and down the chain but cannot cross the muon defect which acts as a barrier. Every time the soliton briefly revisits the muon, the muon-electron hyperfine coupling is turned on and then off, so that successive visits progressively relax the muon polarization. Measurement of the field dependence of this relaxation yields the spectral density function associated with the defect random walk and can be used to infer the dimensionality of the soliton diffusion (Nagamine *et al.* 1984). This occurs because the relaxation rate is connected with the noise power,  $J(\omega_\mu)$ , in the fluctuating magnetic field at the muon Larmor frequency,  $\omega_\mu$ , associated with that particular magnetic field. Sweeping the magnetic field allows one to extract the frequency distribution of the fluctuations. In other polymers, such as polyaniline, the muon-induced defect is a negatively charged polaron. Muons are uniquely sensitive to the motion of this defect in undoped materials (Pratt *et al.* 1997) and in contrast to transport studies, which are inevitably dominated by the slowest component of the transport process, can provide information on the intrinsic transport processes governing the mobility of an electronic excitation along a chain.

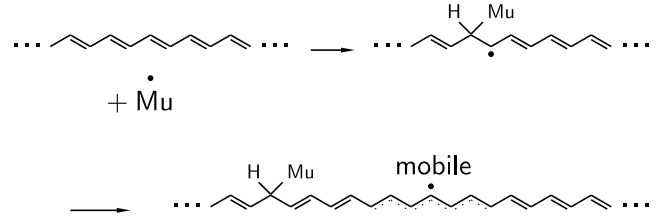


Figure 19: Muonium interaction with trans-polyacetylene to produce a diamagnetic radical and a mobile neutral soliton.

In more conventional materials it is the motion of the muon itself which is of special interest. The dynamics of light atoms such as hydrogen and muonium, or particles such as the proton and muon, are worthwhile to study because they can provide a stringent test for theories on the quantum motion of defects and interstitials (Storchak and Prokof'ev 1998). The smaller mass of the muon leads to larger tunnelling matrix elements to neighbouring sites and thus enhances the quantum mechanical nature of the motion. Furthermore, because muon-muon (or muonium-muonium) interactions can be neglected, the intrinsic nature of the dynamics can be followed without the complications that can be found in studying the corresponding proton or hydrogen case.

In inorganic materials the muon will usually come to rest at an interstitial site. The stability of that site will depend on the depth of the potential well. It is of interest to discover whether local diffusion is possible between interstitial sites. Another process is trapping and release from deep potential wells associated with imperfections or defects. The muon jump rates are found to be about ten times higher than the corresponding proton jump rates, consistent with the lighter muon mass. Hopping is, as expected, assisted by phonons and thus rises with temperature, following an approximately activated behaviour [the hop rates are proportional to  $T^{-1/2} \exp(-E_a/k_B T)$  where  $E_a$  is an activation energy (Flynn and Stoneham 1972)]. This occurs because the muon is initially 'self-trapped' by its own local distortion of the lattice (Figure 20) and a tunnelling transition is only possible if, by the thermal fluctuations of the lattice which occur because of phonons, two neighbouring energy levels coincide [the coincidence configuration, see Figure 20(b)]. The muon can then tunnel through the barrier and becomes self-trapped in the next site.

Lower temperature produces fewer phonons and hence the hop rate falls as the temperature is reduced. However as the temperature is lowered further, a pe-

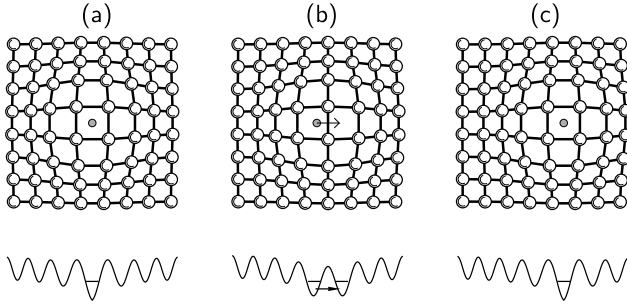


Figure 20: Diffusion process of a muon by phonon-assisted tunnelling. (a) The muon is stable in an interstitial site and the local distortion leads to self-trapping so that its zero-point energy level lies a little lower than the neighbouring site. (b) Thermal fluctuations provide the opportunity for a coincidence configuration whereby tunnelling is allowed, leading to (c) a new stable configuration. (Adapted from Cox *et al.* 1987).

cular effect is observed: the muon hop rate falls to a minimum and then begins to rise again. In the very low temperature regime the phonons appear to be hindering hopping rather than helping it, as they do at higher temperatures. The reason is that at low temperatures coherent tunnelling is possible i.e. the muon is in a band state. Phonons now are responsible for inelastic scattering which destroys the coherence of this delocalized state. This coherent effect is known as quantum diffusion (for a review, see Storchak and Prokof'ev 1998).

Experimental data for various materials are shown in Figure 21 and although there are large differences in the size of the hop rate and the detailed form of the temperature dependence, all show an increasing hop rate at high temperature consistent with activated behaviour and a decreasing hop rate at low temperature consistent with quantum diffusion. An early theoretical treatment of this latter effect predicted that the low temperature hop rate would follow an inverse power law  $T^{-\alpha}$ , where the exponent  $\alpha$  was large, typically  $\sim 9$  (Kagan and Klinger 1974). Experiments on Cu and Al (see Figure 21) showed a more modest behaviour with  $\alpha \sim 0.6-0.7$ . However it was shown that this could be explained by considering the effect of the conduction electrons in a metal, which screen the muon and cannot react fast enough to the diffusing particle and follow it adiabatically. This produces a net drag which reduces the particle hop rate and weakens the temperature dependence. A detailed theory of this effect produces agreement with experiment (Kondo 1984, Yamada 1984, Kagan and Prokof'ev 1986).

This dominant rôle of the electrons has been demonstrated by ingenious experiments on aluminium (Karls-son *et al.* 1995). In its superconducting state, the pres-

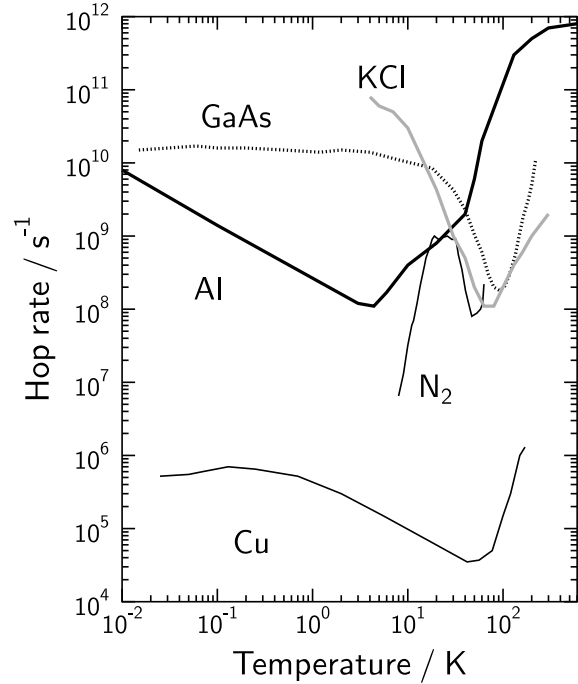


Figure 21: Muon hop rates as a function of temperature for various materials. Copper (Luke *et al.* 1991), aluminium (Hartmann *et al.* 1988), gallium arsenide (Kadono *et al.* 1990), potassium chloride (Kiefl *et al.* 1989), and solid nitrogen (Storchak *et al.* 1994).

ence of the gap in the electronic spectrum effectively decouples the electron bath from the muon. At low temperature the superconductivity can be removed by applying a sufficiently large magnetic field to the sample. This dramatically reduces the muon diffusion rate because the closing of the gap reconnects the muon diffusion process to the electron bath, introducing drag.

In insulators there are no conduction electrons to worry about and in this case the hopping particle is a neutral muonium atom, not a charged muon. The coherent muon hop rate for KCl (Figure 21) rises much more rapidly with decreasing temperature than for metals, and fits to an exponent  $\alpha = 3.3$  (Kiefl *et al.* 1989). This still does not quite fit with the earlier theory (Kagan and Klinger 1974) but agrees with more sophisticated treatments (see Storchak and Prokof'ev 1998) which take into account the measured phonon spectrum in KCl measured using neutron scattering.

In semiconductors muonium is also formed (see section 5) and very similar temperature dependence is found (Figure 21, Kadono *et al.* 1990) with  $\alpha \sim 3$  below 100 K but the hop rate saturates below  $\sim 10$  K due to the presence of disorder. (Below this temperature

the coherent tunnelling is dominated by the disorder, rather than the phonons, and is therefore temperature independent.) Data are also shown for solid nitrogen in Figure 21. This material shows a very sharp increase in hop-rate with decreasing temperature ( $\alpha \sim 7$ , Storchak *et al.* 1994); as the temperature is lowered further it saturates and thereafter begins to decrease. This low temperature effect is thought to be due to orientational ordering of the  $N_2$  molecules but is not yet understood in detail.

## 9 Conclusions

Muons have found extremely wide application in condensed matter physics, allowing physicists and chemists to study a variety of problems concerning magnetism, superconductivity, chemical kinetics, diffusion, molecular dynamics, and semiconductor physics. The interested reader is referred to a number of excellent specialist reviews for further details concerning the technique and its application. (Schenck 1985, Cox 1987, Brewer 1994, Karlsson 1995, Dalmas de Réotier and Yaouanc 1997). Currently there is also active interest in attempting to utilise muons to catalyse fusion (Ponomarev 1990).

The availability of muons at proton sources in various places in the world has led to a great deal of activity in this field. This is because even though the proton source is often designed for some other purpose (the production of neutrons for scattering experiments or the production of mesons for nuclear and particle physics), a muon facility can be “tagged on” for little additional cost. The consequent reduction in proton intensity for the main purpose of the proton source is only a few per cent.

One current limitation of muon techniques is that they require bulk samples because the incident muons are formed with energy 4 MeV and penetrate a few hundred micrometres into any sample. Even with the use of degraders, surface studies have so far not been possible. Recently however there has been considerable progress in the development of so-called ‘slow muon’ beams in which the energy of the muon beam is reduced down to  $\sim 1$ –10 eV. This can be achieved by either moderation in thin layers of rare gas solid (Morenzoni *et al.* 1994) or by resonant ionization of thermal muonium (produced from the surface of a hot tungsten foil placed in a pulsed proton beam) by a pulsed laser source (Nagamine *et al.* 1995). The efficiency of these processes is at present rather too low to allow routine experiments on thin films to take place. Nevertheless as moderator efficiencies improve and the necessary technology is developed, this promises to be a fruitful area of future research.

## References

- Aegerter, C. M., and Lee, S. L., 1997, *Appl. Mag. Res.* **13**, 75.
- Amato, A., 1997, *Rev. Mod. Phys.*, **69**, 1119.
- Anderson, C. D., and Neddermeyer, S. H., 1936, *Phys. Rev.*, **50**, 263.
- Bailey, J., Borer, K., Combley, F., Drumm, H., Krienlen, F., Lange, F., Picasso, E., von Ruden, W., Farley, F. J. M., Field, J. H., Flegel, W., and Hattersley, P. M., 1977, *Nature*, **268**, 301.
- Blatter, G., Feigel'man, M. V., Geshkenbein, V. B., Larkin, A. I., and Vinokur, V. M., 1995, *Rev. Mod. Phys.*, **66**, 1125.
- Blundell, S. J., Pattenden, P. A., Pratt, F. L., Valladares, R. M., Sugano, T., and Hayes, W., 1995, *Europhys. Lett.*, **31**, 573.
- Blundell, S. J., Pratt, F. L., Pattenden, P. A., Kurmoo, M., Chow, K. H., Jestädt, T., and Hayes, W., 1997, *J. Phys.: Condens. Matter*, **9**, 119.
- Brandt, E. H., 1988, *Phys. Rev. B*, **37**, 2349.
- Brewer, J. H., 1994, *Encyclopaedia of Applied Physics* **11**, p23 (VCH, New York).
- Campbell, I. A., Amato, A., Gygax, F. N., Herlach, D., Schenck, A., Cywinski, R., and Kilcoyne, S. H., 1994, *Phys. Rev. Lett.*, **72**, 1291.
- Caso, C., *et al.*, 1998, The 1998 Review of Particle Physics, *Eur. Phys. J.*, **C3**, 1.
- Chaikin, P. M., and Lubensky, T. C., 1995, *Principles of Condensed Matter Physics* Cambridge University Press (1995).
- Chappert, J., 1984, in *Muons and Pions in Materials Research* ed. Chappert, J. and Grynszpan, R. I., (Elsevier, 1984).
- Chow, K. H., Lichti, R. L., Kiefl, R. F., Dunsiger, S., Estle, T. L., Hitti, B., Kadono, R., MacFarlane, W. A., Schneider, J. W., Schumann, D., and Shelley, M., 1994, *Phys. Rev. B*, **50**, 8918.
- Clem, J. R., 1991, *Phys. Rev. B*, **43**, 7837.
- Conversi, M., Pancini, E., and Piccioni, O., 1945, *Phys. Rev.*, **68**, 232.
- Conversi, M., Pancini, E., and Piccioni, O., 1947, *Phys. Rev.*, **71**, 209.
- Cox, S. F. J., 1987, *J. Phys. C*, **20**, 3187.
- Dalmas de Réotier, P., and Yaouanc, A., 1997, *J. Phys.: Condensed Matter*, **9**, 9113.
- Flynn, C. P., and Stoneham, A. M., 1972, *Phys. Rev. B*, **1**, 3966.
- Garwin, R. L., Lederman, L. M., and Weinrich, M., 1957, *Phys. Rev.*, **105**, 1415.
- Hartmann, O., Karlsson, E., Wäckelgård, E., Wappling, R., Richter, D., Hempelmann, R., and Niinikoski, T. O., 1988, *Phys. Rev. B*, **37**, 4425.
- Hayano, R. S., Uemura, Y. J., Imazato, J., Nishida, N., Yamazaki, T., and Kubo, R., 1979, *Phys. Rev. B*, **20**, 850.
- Hayes, W., 1995, *Phil. Trans. R. Soc. Lond. A*, **350**, 249.
- Hess, V. F., 1912, *Phys. Z.*, **13**, 1084.



- Hillier, A. D., and Cywinski, R., 1997, *Appl. Mag. Res.* **13**, 95.
- Kadono, R., Kiefl, R. F., Brewer, J. H., Luke, G. M., Pfiz, T., Riseman, T. M., and Sternlieb, B. J., 1990, *Hyp. Int.*, **64**, 635.
- Kagan, Yu., and Klinger, M. I., 1974, *J. Phys. C*, **7**, 2791.
- Kagan, Yu., and Prokofe'v, N. V., 1986, *JETP*, **63**, 1276.
- Karlsson, E. B., 1995 *Solid State Phenomena*, Oxford.
- Karlsson, E., Wäppling, R., Lidström, S. W., Hartmann, O., Kadono, R., Kiefl, R. F., Hempelmann, R., and Richter, D., 1995, *Phys. Rev. B*, **52**, 6417.
- Keren, A., Le, L. P., Luke, G. M., Sternlieb, B. J., Wu, W. D., Uemura, Y. J., Tajima, S., and Uchida, S., 1993, *Phys. Rev. B*, **48**, 12926.
- Keren, A., Mendels, P., Campbell, I. A., and Lord, J., 1996, *Phys. Rev. Lett.*, **77**, 1386.
- Kiefl, R. F., Kadono, R., Brewer, J. H., Luke, G. M., Yen, H. K., Celio, M., and Ansaldo, E. J., 1989, *Phys. Rev. Lett.*, **53**, 90.
- Kiefl, R. F., Schneider, J. W., MacFarlane, A., Chow, K., Duty, T. L., Estle, T. L., Hitti, B., Lichti, R. L., Ansaldo, E. J., Schwab, C., Percival, P. W., Wei, G., Wlodek, S., Kojima, K., Romanow, W. J., McCauley, J. P., Coustel, N., Fischer, J. E., and Smith, A. B., 1992, *Phys. Rev. Lett.*, **68**, 2708.
- Kojima, K., Keren, A., Luke, G. M., Nachumi, B., Wu, W. D., Uemura, Y. J., Azuma, M., and Takano, M., 1995, *Phys. Rev. Lett.*, **74**, 2812.
- Kondo, J., 1984, *Physica B+C*, **126**, 377.
- Kubo, R., and Toyabe, T., 1967, in *Magnetic Resonance and Relaxation*, ed. Blinc, R., p810, (North-Holland, Amsterdam).
- Lappas, A., Prassides, K., Amato, A., Feyerherm, R., Gy-gax, F. N., and Schenck, A., 1994, *Z. Phys. B*, **96**, 223.
- Lattes, C. M. G., Occhialini, G. P. S., and Powell, C. F., 1947, *Nature*, **160**, 453, 486.
- Le, L. P., Keren, A., Luke, G. M., Sternlieb, B. J., Wu, W. D., Uemura, Y. J., Brewer, J. H., Riseman, T. M., Uspani, R. V., Chiang, L. Y., Kang, W., Chaikin, P. M., Csiba, T., and Grüner, G., 1993, *Phys. Rev. B*, **48**, 7284.
- Lee, S. L., Zimmermann, P., Keller, H., Warden, M., Savić, I. M., Schauwecker, R., Zech, D., Cubitt, R., Forgan, E. M., Kes, P. H., Li, T. W., Menovsky, A. A., and Tarnawski, Z., 1993, *Phys. Rev. Lett.*, **71**, 3862.
- Lee, S. L., Pratt, F. L., Blundell, S. J., Aegerter, C. M., Pattenden, P. A., Chow, K. H., Forgan, E. M., Sasaki, T., Hayes, W., and Keller, H., 1997, *Phys. Rev. Lett.*, **79**, 1563.
- Luke, G. M., Brewer, J. H., Kreitzman, S. R., Noakes, D. R., Celio, M., Kadono, R., and Ansaldo, E. J., 1991, *Phys. Rev. B*, **43**, 3284.
- MacFarlane, W. A., Kiefl, R. F., Dunsiger, S., Sonier, J. E., Chakhalian, J., Fischer, J. E., Yildirim, T., and Chow, K. H., 1998, *Phys. Rev. B*, **58**, 1004.
- Major, J., Mundy, J., Schmolz, M., Seeger, A., Döring, K. P., Fürderer, K., Gladisch, M., Herlach, D., and Majer, G., 1986, *Hyp. Int.*, **31**, 259.
- Morenzoni, E., Kottmann, F., Maden, D., Matthias, B., Meyberg, M., Prokscha, T., Wutzke, T., and Zimmermann, U., 1994, *Phys. Rev. Lett.*, **72**, 2793.
- Nagamine, K., Ishida, K., Matsuzaki, T., Nishiyama, K., Kuno, Y., and Yamazaki, T., 1984, *Phys. Rev. Lett.*, **53**, 1763.
- Nagamine, K., Miyake, Y., Shimomura, K., Birrer, P., Iwasaki, M., Strasser, P., and Kuga, T., 1995, *Phys. Rev. Lett.*, **74**, 4811.
- Patterson, B. D., 1988, *Rev. Mod. Phys.*, **60**, 69.
- Ponomarev, L. I., 1990, *Contemp. Phys.*, **31**, 219.
- Pratt, F. L., 1997, *Phil. Mag. Lett.*, **75**, 371.
- Pratt, F. L., Blundell, S. J., Hayes, W., Ishida, K., Nagamine, K., and Monkman, A. P., 1997, *Phys. Rev. Lett.*, **79**, 2855.
- Reid, I. D., Azuma, T., and Roduner, E., 1990, *Nature*, **345**, 328.
- Roduner, E., 1993, *Chem. Soc. Rev.*, **22**, 337.
- Rossi, B., and Hall, D. B., 1941, *Phys. Rev.*, **59**, 223.
- Schenck, A., and Gy-gax, F. N., 1995, in *Handbook of Magnetic Materials* 9 edited by Buschow, K. H. J., (Elsevier).
- Schenck, A., 1985, *Muon Spin Rotation: Principles and Applications in Solid State Physics* (Adam Hilger, Bristol).
- Sonier, J. E., Kiefl, R. F., Brewer, J. H., Bonn, D. A., Carolan, J. F., Chow, K. H., Dosanjh, P., Hardy, W. N., Liang, R., MacFarlane, W. A., Mendels, P., Morris, G. D., Riseman, T. M., and Schneider, J. W., 1994, *Phys. Rev. Lett.*, **72**, 744.
- Sonier, J. E., Brewer, J. H., Kiefl, R. F., Bonn, D. A., Dunsiger, S. R., Hardy, W. N., Liang, R., MacFarlane, W. A., Miller, R. I., Riseman, T. M., Noakes, D. R., Stronach, C. E., and White Jr., M. F., 1997, *Phys. Rev. Lett.*, **79**, 2875.
- Storchak, V. G., Brewer, J. H., and Morris, G. D., 1994, *Phys. Lett. A*, **193**, 199.
- Storchak, V. G., and Prokof'ev, N. V., 1998, *Rev. Mod. Phys.*, **70**, 929.
- Uemura, Y. J., Yamazaki, T., Harshman, D. R., Senba, M., and Ansaldo, E. J., 1985, *Phys. Rev. B*, **31**, 546.
- Uemura, Y. J., Le, L. P., Luke, G. M., Sternlieb, B. J., Wu, W. D., Brewer, J. H., Riseman, T. M., Seaman, C. L., Maple, M. B., Ishikawa, M., Hinks, D. G., Jorgensen, J. D., Saito, G., and Yamochi, H., 1991, *Phys. Rev. Lett.*, **66**, 2665.
- Uemura, Y. J., Keren, A., Kojima, K., Le, L. P., Luke, G. M., Wu, W. D., Ajiro, Y., Asano, T., Kuriyama, Y., Mekata, M., Kikuchi, H., and Kakurai, K., 1994, *Phys. Rev. Lett.*, **73**, 3306.
- Wulf, T., 1910, *Phys. Z.*, **10**, 811.
- Yamada, K., 1984, *Prog. Theor. Phys.*, **72**, 195.
- Yaouanc, A., Dalmas de Réotier, P., and Brandt, E. H., 1997, *Phys. Rev. B*, **55**, 11107.
- Xu, Q., and Brown, L. M., 1987, *Amer. J. Phys.*, **55**, 23.